Functional Materials

DOI: 10.1002/anie.201405145

Self-Healable Electrically Conducting Wires for Wearable Microelectronics**

*Hao Sun, Xiao You, Yishu Jiang, Guozhen Guan, Xin Fang, Jue Deng, Peining Chen, Yongfeng Luo, and Huisheng Peng**

Abstract: *Electrically conducting wires play a critical role in the advancement of modern electronics and in particular are an important key to the development of next-generation wearable microelectronics. However, the thin conducting wires can easily break during use, and the whole device fails to function as a result. Herein, a new family of high-performance conducting wires that can self-heal after breaking has been developed by wrapping sheets of aligned carbon nanotubes around polymer fibers. The aligned carbon nanotubes offer an effective strategy for the self-healing of the electric conductivity, whereas the polymer fiber recovers its mechanical strength. A self-healable wire-shaped supercapacitor fabricated from a wire electrode of this type maintained a high capacitance after breaking and self-healing.*

Electrically conducting wires with excellent mechanical and electrical properties are in high demand for the rapid development of modern electronics, in particular, wearable devices and products.[1,2] As compared with conventional metal wires, these new conducting wires are required to be more lightweight with higher surface areas.[3] A wide variety of nanomaterials, such as carbon nanotubes (CNTs)[4–8] and Ag nanowires,[9,10] have been proposed as promising candidates. For example, CNTs, which are widely studied for their combined remarkable electronic, mechanical, and thermal properties, have been made into continuous fibers with high electrical conductivities that are attractive for portable and wearable electronic devices.[7,8] However, these nanomaterial-based micrometer-sized fibers appear to have a common critical problem: They easily break under bending or other deformations that often occur during use, and the whole device fails to function as a result.[8] This problem will be solved if the conducting CNT fiber can be healed to restore its electrical and mechanical properties after breaking.

[*] H. Sun, X. You, Y. Jiang, G. Guan, X. Fang, J. Deng, P. Chen, Dr. Y. Luo, Prof. H. Peng
State Key Laboratory of Molecular Engineering of Polymers
Department of Macromolecular Science and
Laboratory of Advanced Materials, Fudan University
Shanghai 200438 (China)
E-mail: penghs@fudan.edu.cn

[**] This research was supported by the NSFC (21225417), MOST (2011CB932503), STCSM (12nm0503200), the Fok Ying Tong Education Foundation, the Program for Professors of Special Appointment at Shanghai Institutions of Higher Learning, and the Program for Outstanding Young Scholars from the Organization Department of the CPC Central Committee.

Supporting information for this article is available on the WWW under http://dx.doi.org/10.1002/anie.201405145.

The development of wire-shaped energy-storage devices is a promising, mainstream direction in the field of wearable and portable electronics.[11,12] As compared with the conventional planar structure, the wire shape enables many unique and promising advantages, particularly, the ability to be woven into lightweight, soft, and flexible energy textiles.[2,11–15] Wire-shaped devices are generally microdevices, typically with diameters of tens of micrometers to a few millimeters. Such chemical fibers meet the weaving requirements in the textile industry. In an energy textile woven from wire-shaped devices, the thin device is susceptible to structure fracture under bending or during energy conversion and storage processes;[8,12] the fiber electrode also undergoes mechanical damage caused by deformations or accidental cutting during use. As a result, the whole energy textile may fail to work or may only function with low efficiency. Therefore, the lifetime of the wire-shaped device becomes very low in practical applications, which remains a challenge for the future development of wire-shaped electronics.

Herein, we describe the development of a new family of self-healable conducting wires by the wrapping of electrically conducting nanomaterials, such as CNTs and Ag nanowires, around polymer fibers. The excellent electrical and mechanical properties are recovered by the one-dimensional nanomaterials in the sheath and the polymer fiber in the core after breaking and self-healing. As a demonstration of their application, the self-healable core–sheath wires were used to fabricate a novel wire-shaped supercapacitor. A high specific capacitance of $140.0\,F\,g^{-1}$ or $1.34\,mF\,cm^{-1}$ was produced and recovered to 92% after the self-healing of a broken wire-shaped supercapacitor.

The structure of the self-healable conducting wire is shown schematically in Figure 1. The self-healing polymer (SHP; see the chemical structure in Figure S1 of the Supporting Information) was synthesized by a procedure derived from the Leibler method.[16] The resulting fibers typically showed a diameter of approximately 700 μm. Three conducting materials were studied as the conducting layer: aligned-carbon-nanotube sheets, Ag nanowires, and a carbon-nanotube network. Aligned-CNT sheets were dry-drawn from a spinnable CNT array (see Figure S2). The thickness of the CNT sheet could be controlled from 0.15 to 0.59 μm by varying the layer number. The resulting CNT film was then scrolled onto a SHP fiber (see Figure S3). The cross-sectional view by scanning electron microscopy (SEM) verified that the aligned-CNT layer was closely and uniformly attached to the SHP fiber (see Figure S4), which is important for the electrical self-healing of the electrode. The CNTs remained highly aligned along the axial direction to enable high

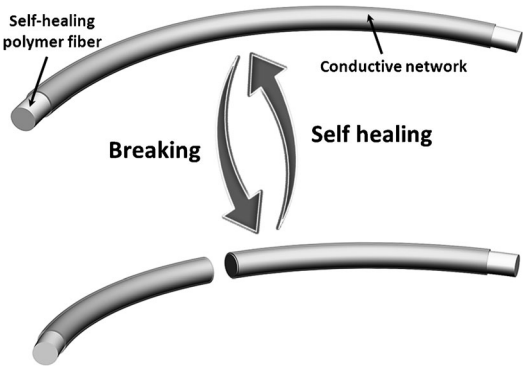

Figure 1. Schematic illustration of the self-healing of the conducting wire.

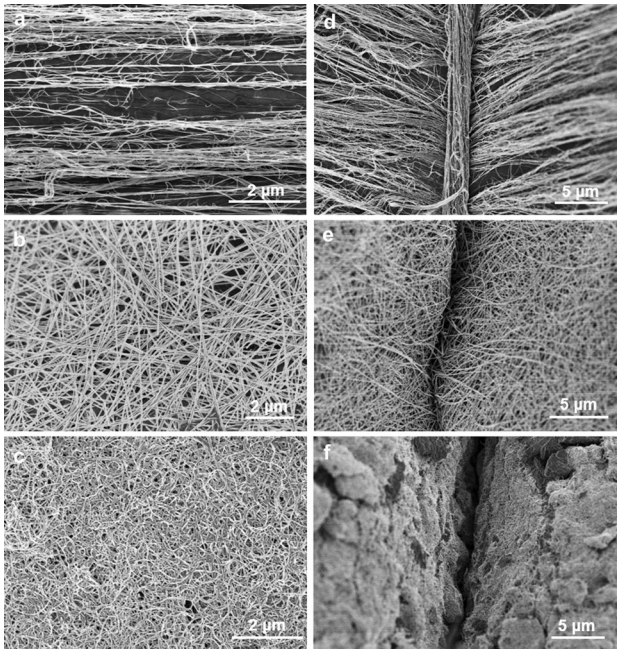

Figure 2. SEM images of three self-healable fibers. a,d) A CNT-sheet-based fiber before breaking and after self-healing, respectively. b,e) A silver-nanowire-based fiber before breaking and after self-healing, respectively. c,f) A CNT-network-based fiber before breaking and after self-healing, respectively.

electrical conductivity (Figure 2a). For the other two wire types, Ag nanowires and CNTs were dispersed in ethanol and then spray-coated on the surface of the SHP fiber, whereupon the Ag nanowires and CNTs aggregated into network structures (Figure 2b,c).

The core–sheath conducting wires based on the aligned-CNT sheet, Ag nanowires, and CNT networks all underwent self-healing of their structure after breaking. Figure 2d–f shows typical SEM images of the "scar" after cutting and self-healing for the different conducting layers. In the case of the aligned-CNT sheet, an aligned-CNT strand was formed along the cross-sections of all broken ends during the cutting process (Figure 2d). The strand was found to serve as a "bridge" to connect the two broken ends of the CNTs upon contacting, which is favorable for the self-healing of an electrical property, such as electrical conductivity of the fiber, and is discussed below. In contrast, no strands were observed for the randomly dispersed Ag nanowires and CNT networks at the breaking point (Figure 2e,f).

The mechanical and electrical properties of the three conducting wires before breaking and after self-healing were further compared. The tensile strengths were close and were maintained typically at approximately 80%, but at up to 92% (Figure 3a). The electrical resistance was measured to be 140, 12, and $5.7\times10^{3}\ \Omega\,cm^{-1}$ for conducting wires based on the aligned-CNT sheet, the silver-nanowire network, and the CNT network, respectively, with the same length of 5 cm. As expected, Ag nanowires produced the lowest resistance. The aligned-CNT sheet also showed low resistance suitable for applications in electronics owing to the aligned arrangement of the CNTs, and electrons were efficiently transported along the length of the CNTs. In contrast, a very high resistance was produced by the CNT network, in which electrons have to hop over many boundaries and contacting points. Upon self-healing of the three conducting wires, the resistance was increased by 8.5, 191.6, and 176.5% for the wires based on the aligned CNT sheet, the silver-nanowire network, and the CNT network, respectively (Figure 3b). The changes in resistance are also critical to the practical application of these materials as self-healable conducting wires. The resistance was increased by 60, 115, and $5.0\times10^{4}\ \Omega$ after breaking and self-healing for the aligned-CNT sheet, the silver-nanowire network, and the CNT network, respectively. Conduct-

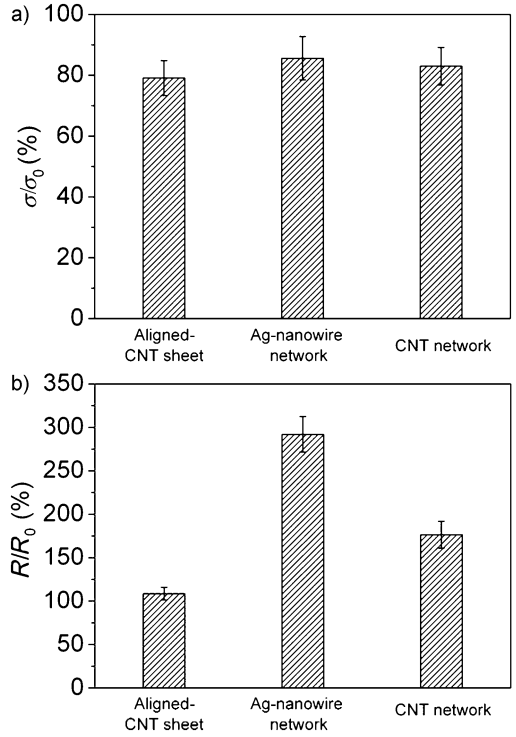

Figure 3. Comparison of the mechanical and electrical properties of three conducting wires after self-healing. a) Tensile strength: σ_0 and σ correspond to the strength before breaking and after self-healing, respectively. b) Electrical resistance: R_0 and R correspond to the resistance before breaking and after self-healing, respectively.

ing wires derived from the aligned-CNT sheet and the silver-nanowire network showed a relatively low increase in resistance. On the basis of the above comparison, the aligned-CNT sheet is mainly considered in the following discussion.

The mechanical and electrical self-healing properties of aligned-CNT/SHP fibers were systematically investigated. Figure 4a shows stress–strain curves of a fiber before breaking and after self-healing. The strengths were maintained at 79.1 and 72.5% after self-healing for one and five cycles, respectively. The dependence of the mechanical recovery on the thickness of the wound in the CNT film was also investigated by comparing the tensile strengths before breaking and after self-healing (see Figure S7). The tensile strengths were maintained and fluctuated at around 80% in the thickness range up to 0.59 μm. The high self-healing with respect to electrical conductivity was further verified by the resistance maintained after self-healing (Figure 4b). Upon breaking, the resistance of a CNT/SHP fiber with a length of approximately 1.5 cm was increased from about 200 to over 10^7 Ω. After the two broken cross-sections regained contact, the resistance was recovered to approximately 600 Ω as a result of the reconstruction of the conducting CNT layer on the surface. The resistance was further decreased to 250 Ω when the two contacted cross-sections were gently pressed together. When the broken parts are brought back into contact, hydrogen bonds are formed between the two sections of the SHP fiber to connect them together; at the same time, the aligned CNTs between the two cross-sections are reconnected by van der Waals forces during the self-healing process of the SHP fiber. It was previously found that a high adhesive force was produced between aligned CNT arrays and various substrates by van der Waals interactions.[17] Although van der Waals forces are weak, the collective effect from a lot of CNTs with a number-density range of approximately 10^{10}–10^{11} cm^{-2} produces a high adhesive force. Similarly, aligned-CNT sheets have the same number density as the CNT array, and the large number of aligned CNTs enables an effective connection across the breaking point. A pressing force from the two sides enhances the hydrogen bonds and the van der Waals force with a better self-healing effect. The reversible breaking and healing processes could be repeated well with satisfying performances (Figure 4c).

Figure 5 shows an effective application of the self-healing fiber as a conducting wire to power a light-emitting diode (LED) in a circuit. In this case, the thickness of the aligned-CNT sheet was 0.27 μm, and the LED lamp successfully lighted up at a voltage of 3.0 V (Figure 5a). After breaking of

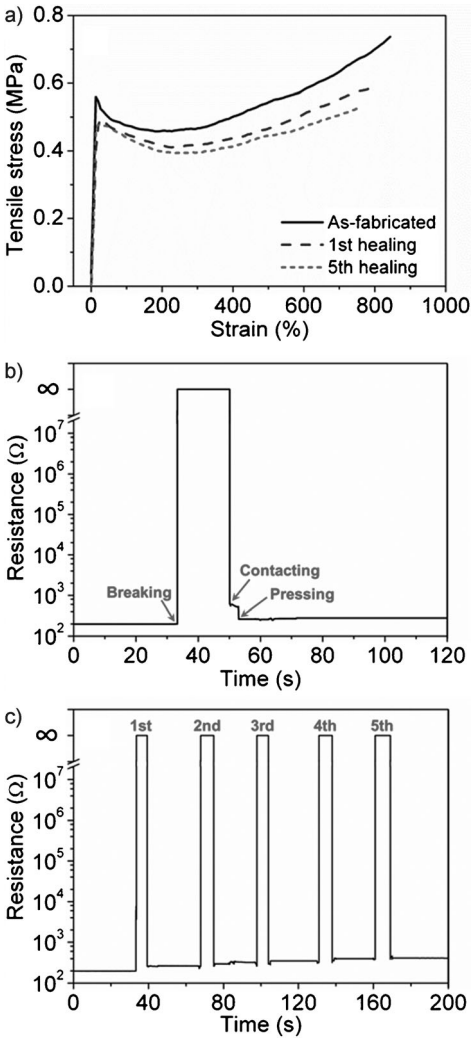

Figure 4. Mechanical and electrical properties of the aligned-CNT/SHP fiber before breaking and after healing. a) Stress–strain curves of an as-prepared fiber and the fiber after one and five cycles of breaking/healing. b) Electrical resistance of a fiber before breaking, after breaking, and after healing. c) Electrical resistance in five breaking/self-healing cycles.

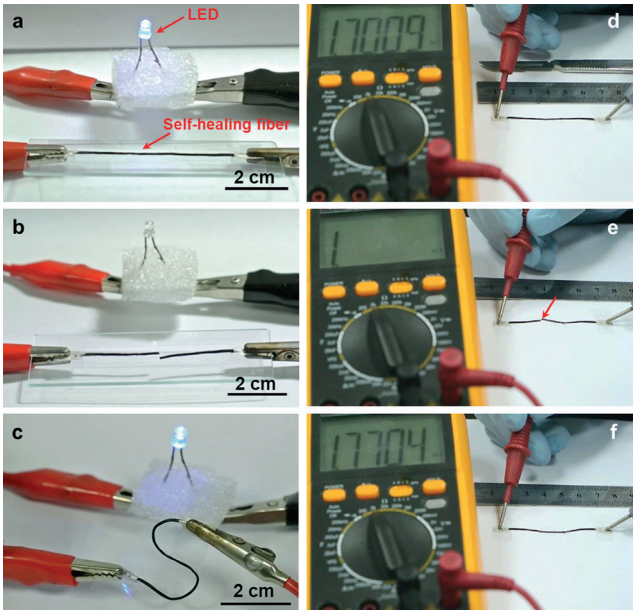

Figure 5. a,b,c) Photographs of a self-healing fiber serving as a conducting wire to power a LED before breaking, after breaking, and after healing and being bent, respectively. The voltage was set at 3.2 V. d,e,f) Electrical resistance of a fiber with a length of 5 cm before breaking, after breaking, and after healing, respectively. The red arrow in (e) indicates the breaking position. The unit of the resistance displayed on the multimeter was kΩ.

the CNT/SHP fiber, the LED turned off (Figure 5b). The LED lamp was lit up again with almost the same brightness after self-healing of the fiber (Figure 5c). Furthermore, no obvious damage was found, and the brightness of the LED lamp was also maintained by bending the "scar" part of the self-healed fiber, thus indicating high self-healing performance in terms of both mechanical and electrical properties (Figure 5c). The resistance of the CNT/SHP fiber with a length of 5 cm was also traced by a multimeter and increased slightly by approximately 5% after self-healing (Figure 5d–f).

The remarkable mechanical and electrical performance makes the self-healing fiber promising for various electronic applications. As a demonstration, a self-healable wire-shaped supercapacitor was fabricated by twisting two CNT/SHP fibers as electrodes with a poly(vinyl alcohol)–H_2SO_4 gel electrolyte that also served as the separator (see Figure S9). Cyclic voltammetry (CV) was first conducted with CNT films of increasing thickness at the same length of 1.2 cm and a scan rate of 100 $mV\,s^{-1}$ (see Figure S10). The area of the CV curve that corresponded to the capacitance was first increased with increasing thickness from 0.15 to 0.38 μm and then reached a plateau with a further increase in thickness. The plateau may be explained by the fact that the gel electrolyte can only penetrate into a specific thickness range of CNT films. The graph in Figure 6a compares the specific capacitance based on different thicknesses of the CNT film. A maximal specific capacitance of 11.1 $F\,g^{-1}$ was observed at 0.38 μm, as expected. The specific capacitance was calculated from the mass of the active material in the electrode. Electrochemical impedance spectroscopy was also used to study the interface and charge transfer in the wire-shaped supercapacitor (see Figure S11). The near 90° inclination of the Nyquist plot showed pure capacitor behavior.[14,18] The equivalent series resistance decreased from 1.50 to 0.86 kΩ with increasing CNT thickness from 0.15 to 0.38 μm and then decreased slightly to 0.75 kΩ with a further increase to 0.47 μm; that is, thicker CNT films exhibited lower charge-transfer resistance. On the basis of the above comparison, a CNT-film thickness of 0.38 μm is mainly considered in the following discussion.

The well-retained symmetrical triangle shape of typical galvanostatic charge–discharge curves (Figure 6b) and the rectangular shape of the CV curve (see Figure S12) of the wire-shaped supercapacitor show its high stability, which was also verified by its high rate performance (see Figure S13). The Coulombic efficiency was decreased when the current density returned to 0.08 $A\,g^{-1}$ at 40–50 cycles. At a high current density, the electrode was polarized to produce a large overpotential. As a result, the splitting potential of water became high, thus leading to a high Coulombic efficiency. When the current density was decreased, the electrode polarization became weak, and the overpotential was decreased, which resulted in the splitting of water (H_2 evolution at the negative electrode and O_2 evolution at the positive electrode) with lower Coulombic efficiency.

Figure 6c compares galvanostatic charge–discharge curves of a wire-shaped supercapacitor before breaking and

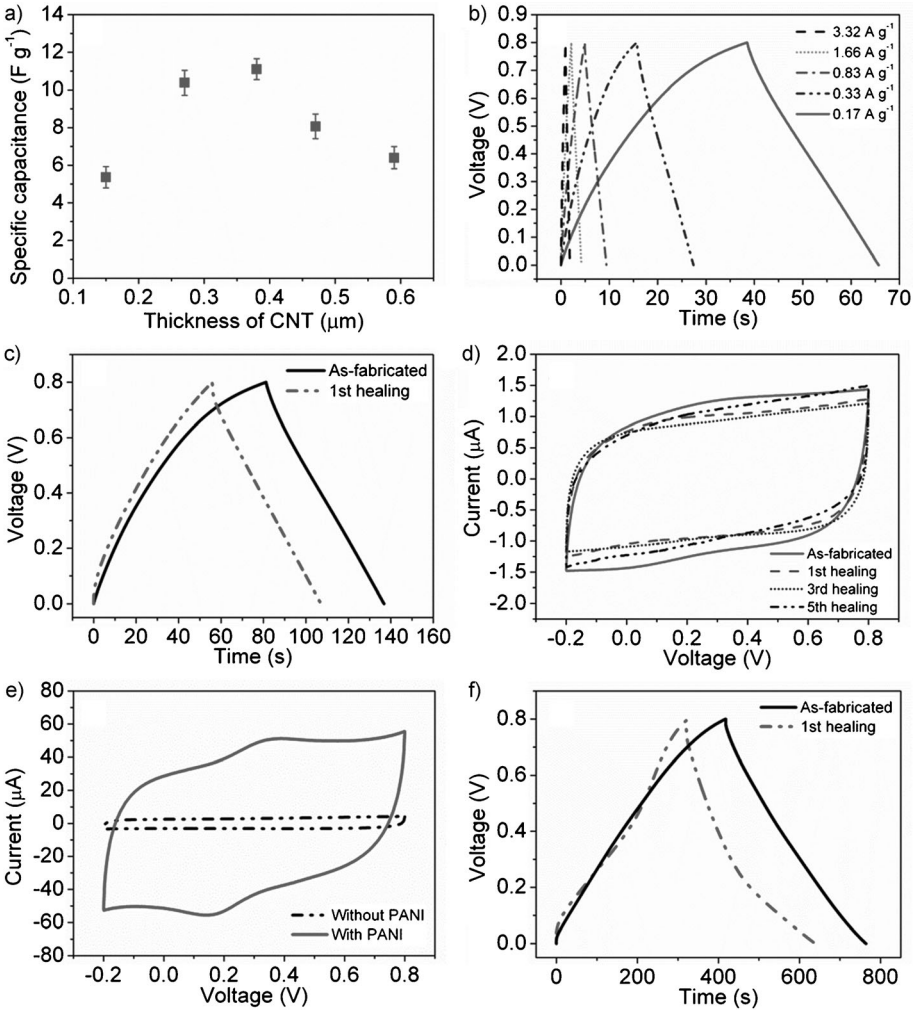

Figure 6. a) Dependence of the specific capacitance on the thickness of the aligned-CNT film. b) Galvanostatic charge–discharge curves of a wire-shaped supercapacitor with increasing current densities at a CNT thickness of 0.38 μm. c) Galvanostatic charge–discharge curves of a wire-shaped supercapacitor before breaking and after healing at a current density of 0.08 $A\,g^{-1}$. d) CV curves of a wire-shaped supercapacitor at a scan rate of 50 $mV\,s^{-1}$ after 1, 3, and 5 healing cycles. e) CV curves of wire-shaped supercapacitors based on aligned-CNT/SHP fibers before and after the incorporation of PANI. f) Galvanostatic charge–discharge curves of the wire-shaped supercapacitor containing PANI before breaking and after healing at a current density of 0.17 $A\,g^{-1}$.

after self-healing at a current density of 0.08 $A g^{-1}$. Importantly, the triangle remained symmetrical, and the discharge time was also close after self-healing to that observed prior to breaking. The equivalent series resistance was increased from 1.30 to 3.02 kΩ after healing (see Figure S14). The CV shapes were also maintained at a scan rate of 50 $mV s^{-1}$ after increasing numbers of healing cycles (Figure 6d), and the specific capacitance was maintained at approximately 82.6% after the fifth healing cycle. Furthermore, the specific capacitance of the self-healed wire-shaped supercapacitor was well maintained in 2000 charge–discharge cycles at a current density of 0.17 $A g^{-1}$, thus demonstrating a high cyclic stability after healing (see Figure S15).

The electrochemical properties of the self-healable wire-shaped supercapacitors could be further improved by introducing a second active phase, such as a conducting polymer. Thus, polyaniline (PANI) was uniformly incorporated into aligned CNTs through electropolymerization (see Figure S16).[19] Wire-shaped supercapacitors with the same amount of PANI and different CNT thicknesses of 0.27 and 0.38 μm were compared. The capacitance was almost the same in each case, but the former material showed a higher specific capacitance owing to the presence of fewer CNTs. Therefore, a thickness of 0.27 μm is mainly considered below. A PANI/CNT mass ratio of 1:1 was mainly studied for the self-healable wire-shaped supercapacitor. Figure 6e compares CV curves of two supercapacitors without and with the incorporation of PANI at a scan rate of 100 $mV s^{-1}$. A pair of redox peaks between 0.1 and 0.4 V indicate a pseudocapacitance derived from PANI that enabled a higher specific capacitance to be reached. The high electrochemical performance upon the incorporation of PANI was also demonstrated by CV and galvanostatic charge–discharge curves. The CV curves retained their shape with increasing scan rates (see Figure S17), and the symmetrical triangle in the galvanostatic charge–discharge curves was well maintained with increasing current densities from 0.17 to 3.32 $A g^{-1}$ (see Figure S18). A high specific capacitance of 140.0 $F g^{-1}$ (1.34 $mF cm^{-1}$) was observed at 0.33 $A g^{-1}$. The introduction of PANI was not detrimental to the self-healing performance, and the specific capacitance was maintained at up to 92% after one self-healing process (Figure 6f). The specific capacitance was maintained at approximately 86% after 1000 charge–discharge cycles at 1.66 $A g^{-1}$ after healing (see Figure S19).

Three self-healable wire-shaped supercapacitors were connected in series to power a LED. The supercapacitors could successfully power the LED (Figure 7a), and then could not power the LED after breaking (Figure 7b). As expected, the wire-shaped supercapacitor could light up the LED again with almost the same brightness after self-healing (Figure 7c).

In conclusion, a new family of self-healable conducting wires has been developed by coating electrically conducting nanomaterials on the surface of polymer fibers. These conducting wires can efficiently recover the high electrical conductivity and mechanical strength of the coated nanomaterial layer in the sheath and polymer fiber in the core, respectively. The self-healable conducting wires were used to fabricate novel wire-shaped supercapacitors, whose high specific capacitance of 140.0 $F g^{-1}$ or 1.34 $mF cm^{-1}$ was restored to 92% after self-healing. The self-healable conducting wires and resulting wire-shaped energy devices are particularly promising for wearable and portable electronics.

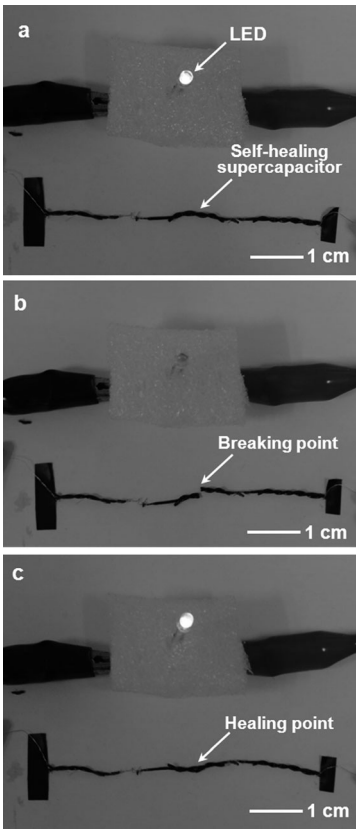

Figure 7. Photographs of three wire-shaped supercapacitors connected in series to power a LED lamp a) before breaking, b) after breaking, and c) after healing.

Received: May 9, 2014
Published online: July 14, 2014

Keywords: carbon nanotubes · conducting wires · microelectronics · polymers · self-healing

[1] G. Xu, J. Zhao, S. Li, X. Zhang, Z. Yong, Q. Li, *Nanoscale* **2011**, *3*, 4215–4219.
[2] Z. Yang, J. Deng, X. Chen, J. Ren, H. Peng, *Angew. Chem.* **2013**, *125*, 13695–13699; *Angew. Chem. Int. Ed.* **2013**, *52*, 13453–13457.
[3] X. Zhang, Q. Li, T. G. Holesinger, P. N. Arendt, J. Huang, P. D. Kirven, T. G. Clapp, R. F. DePaula, X. Liao, Y. Zhao, *Adv. Mater.* **2007**, *19*, 4198–4201.
[4] Q. Li, X. Zhang, R. F. DePaula, L. Zheng, Y. Zhao, L. Stan, T. G. Holesinger, P. N. Arendt, D. E. Peterson, Y. T. Zhu, *Adv. Mater.* **2006**, *18*, 3160–3163.
[5] F. Meng, X. Zhang, R. Li, J. Zhao, X. Xuan, X. Wang, J. Zou, Q. Li, *Adv. Mater.* **2014**, *26*, 2480–2485.
[6] N. Behabtu, C. C. Young, D. E. Tsentalovich, O. Kleinerman, X. Wang, A. W. Ma, E. A. Bengio, R. F. ter Waarbeek, J. J. de Jong, R. E. Hoogerwerf, *Science* **2013**, *339*, 182–186.

[7] T. Chen, S. Wang, Z. Yang, Q. Feng, X. Sun, L. Li, Z. S. Wang, H. Peng, *Angew. Chem.* **2011**, *123*, 1855 – 1859; *Angew. Chem. Int. Ed.* **2011**, *50*, 1815 – 1819.
[8] H. Sun, X. You, J. Deng, X. Chen, Z. Yang, P. Chen, X. Fang, H. Peng, *Angew. Chem.* **2014**, DOI: 10.1002/ange.201403168; *Angew. Chem. Int. Ed.* **2014**, DOI: 10.1002/anie.201403168.
[9] L. Hu, H. S. Kim, J.-Y. Lee, P. Peumans, Y. Cui, *ACS Nano* **2010**, *4*, 2955 – 2963.
[10] S. Yun, X. Niu, Z. Yu, W. Hu, P. Brochu, Q. Pei, *Adv. Mater.* **2012**, *24*, 1321 – 1327.
[11] Y. N. Meng, Y. Zhao, C. G. Hu, H. H. Cheng, Y. Hu, Z. P. Zhang, L. T. Qu, *Adv. Mater.* **2013**, *25*, 2326 – 2331.
[12] J. Ren, L. Li, C. Chen, X. Chen, Z. Cai, L. Qiu, Y. Wang, X. Zhu, H. Peng, *Adv. Mater.* **2013**, *25*, 1155 – 1159.
[13] H. Cheng, J. Liu, Y. Zhao, H. G. Hu, Z. P. Zhang, N. Chen, L. Jiang, L. T. Qu, *Angew. Chem.* **2013**, *125*, 10676 – 10680; *Angew. Chem. Int. Ed.* **2013**, *52*, 10482 – 10486.
[14] H. Sun, X. You, J. Deng, X. Chen, Z. Yang, J. Ren, H. Peng, *Adv. Mater.* **2014**, *26*, 2868 – 2873.
[15] J. Bae, M. K. Song, Y. J. Park, J. M. Kim, M. Liu, Z. L. Wang, *Angew. Chem.* **2011**, *123*, 1721 – 1725; *Angew. Chem. Int. Ed.* **2011**, *50*, 1683 – 1687.
[16] P. Cordier, F. Tournilhac, C. Soulié-Ziakovic, L. Leibler, *Nature* **2008**, *451*, 977 – 980.
[17] L. Qu, L. Dai, M. Stone, Z. Xia, Z. L. Wang, *Science* **2008**, *322*, 238 – 242.
[18] M. Yu, Y. Zeng, C. Zhang, X. Lu, C. Zeng, C. Yao, Y. Yang, Y. Tong, *Nanoscale* **2013**, *5*, 10806 – 10810.
[19] H. Lin, L. Li, J. Ren, Z. Cai, L. Qiu, Z. Yang, H. Peng, *Sci. Rep.* **2013**, *3*, 1353.

